MolecularMedicine

Long-term Safety and Efficacy of Human-Induced Pluripotent Stem Cell (iPS) Grafts in a Preclinical Model of Retinitis Pigmentosa

Yao Li,[1,2] Yi-Ting Tsai,[1,2*] Chun-Wei Hsu,[1,2] Deniz Erol,[1,2] Jin Yang,[1,2] Wen-Hsuan Wu,[1,2] Richard J Davis,[1,2] Dieter Egli,[3] and Stephen H Tsang[1,2,4,5]*

[1]Bernard & Shirlee Brown Glaucoma Laboratory, Columbia University; [2]Department of Ophthalmology, Columbia University; [3]The New York Stem Cell Foundation Laboratory; and the [4]Department of Pathology and Cell Biology, Columbia University, New York, New York, United States of America; [5]Columbia University Medical Center/New York Presbyterian Hospital, New York, New York, United States of America

The U.S. Food and Drug Administration recently approved phase I/II clinical trials for embryonic stem (ES) cell–based retinal pigmented epithelium (RPE) transplantation, but this allograft transplantation requires lifelong immunosuppressive therapy. Autografts from patient-specific induced pluripotent stem (iPS) cells offer an alternative solution to this problem. However, more data are required to establish the safety and efficacy of iPS transplantation in animal models before moving iPS therapy into clinical trials. This study examines the efficacy of iPS transplantation in restoring functional vision in *Rpe65*^{rd12}/*Rpe65*^{rd12} mice, a clinically relevant model of retinitis pigmentosa (RP). Human iPS cells were differentiated into morphologically and functionally RPE-like tissue. Quantitative real-time polymerase chain reaction (RT-PCR) and immunoblots confirmed RPE fate. The iPS-derived RPE cells were injected into the subretinal space of *Rpe65*^{rd12}/*Rpe65*^{rd12} mice at 2 d postnatally. After transplantation, the long-term surviving iPS-derived RPE graft colocalized with the host native RPE cells and assimilated into the host retina without disruption. None of the mice receiving transplants developed tumors over their lifetimes. Furthermore, electroretinogram, a standard method for measuring efficacy in human trials, demonstrated improved visual function in recipients over the lifetime of this RP mouse model. Our study provides the first direct evidence of functional recovery in a clinically relevant model of retinal degeneration using iPS transplantation and supports the feasibility of autologous iPS cell transplantation for retinal and macular degenerations featuring significant RPE loss.

Online address: http://www.molmed.org
doi: 10.2119/molmed.2012.00242

INTRODUCTION

Among the elderly, blindness is feared more than any illness besides cancer. Diseases caused by retinal pigmented epithelium (RPE) malfunction, including age-related macular degeneration (AMD) and some forms of retinitis pigmentosa (RP), afflict at least 8 million Americans, leading to vision loss, functional impairment and physical and psychological hardship. As the average lifespan increases, disease prevalence is expected to rise. Treatments such as ranibizumab show the capacity to slow the rate of vision loss, but have no more than a 10% rate of effectiveness in all AMD cases (1). No other treatments are currently available to restore the vision of patients who suffer from RPE loss.

The year 2011 brought a new advance in the treatment of macular degenerations, with the U.S. Food and Drug Administration approving clinical trials using ES cell–derived retinal pigment epithelium (RPE) transplants (2). The eye is an ideal testing ground for stem cell therapies, since it exhibits relative immune privilege, it is readily accessible for monitoring and imaging purposes and in the event of serious complications, its removal is not a life-threatening event.

Our current study focuses on induced pluripotent stem (iPS) cells, which offer a compelling alternative approach for stem cell therapy. iPS cells can provide potentially unlimited autologous cells for functional testing and optimization. They render immunosuppression unnecessary after transplantation. Recent studies point to their promise, finding that iPS cell–derived RPE cells are more akin to primary fetal RPE than immortal RPE cell lines in terms of morphology, gene expression and immunohistochemical

*YL and Y-TT contributed equally to this work.

Address correspondence to *Stephen H Tsang, Edward Harkness Eye Institute, 160 Fort Washington Avenue, Research Annex, Room 513, New York, NY 10032. Phone: 212-342-1189; Fax: 212-305-4987; E-mail: sht2@columbia.edu.*

Submitted June 7, 2012; Accepted for publication August 9, 2012; Epub (www.molmed.org) ahead of print August 9, 2012.

The Feinstein Institute for Medical Research North Shore LIJ

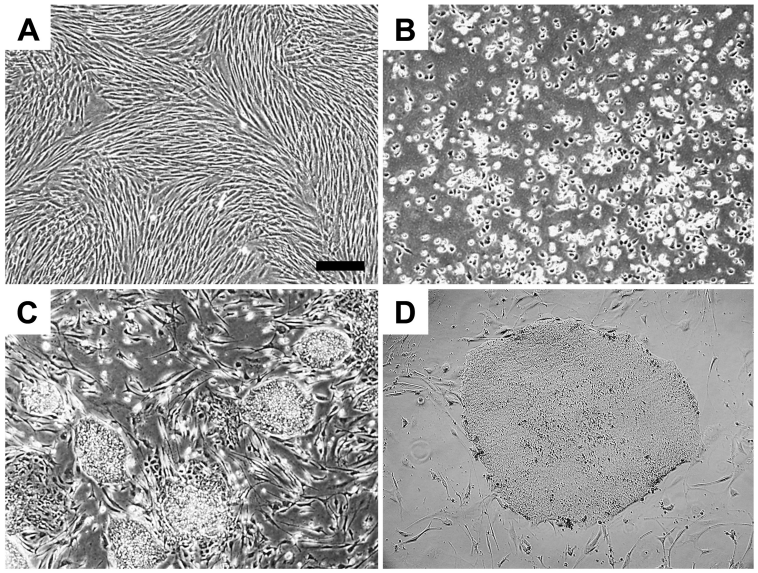

Figure 1. Generation of human iPS cell lines from skin fibroblasts. (A) Fibroblast monolayer. (B, C) Fibroblasts after transduction with *OCT4, SOX2, KLF4* and *MYC*. iPS colonies appeared between 14 and 21 d (4×). (D) iPS colony (10×). Scale bar, 100 μm.

analysis (3). Other studies have documented native RPE transplants' ability to improve electroretinogram (ERG) function in the Royal College of Surgeons (RCS) rat model of RP (4,5).

Previous reports on iPS cell–derived RPE transplantation show enhanced visual guided behavior but not enhanced ERGs in RCS rats for 6 wks after transplantation (6). Hence, future studies must validate the efficacy of iPS transplants with the ERG, the universally accepted standard for objective assessment of visual function in humans (7,8). Benchmarks for efficacy and safety must be established in a preclinical model before moving on to human studies.

The current study tested both the safety of differentiating human iPS cells into RPE for implant and the efficacy of iPS transplantation in improving retinal function in the $Rpe65^{rd12}/Rpe65^{rd12}$ mouse. In addition, to determine whether any rescue effects were due to surgical injury or feeder cells, control groups of $Rpe65^{rd12}/Rpe65^{rd12}$ mice received grafts of mitomycin-C–treated undifferentiated mouse ES cells. Encouragingly, the iPS cell–derived RPE cells expressed RPE markers, and the mice transplanted with these cells showed enhanced ERG responses compared with control groups.

MATERIALS AND METHODS

Human Samples and Mice

Institutional Review Board approval IRB-AAAF1849 was obtained from Columbia University Medical Center/New York Presbyterian Hospital, and all research procedures adhered to the tenets of the Declaration of Helsinki. Informed consent was obtained from all subjects in the study, and Health Insurance Portability and Accountability Act compliance was maintained. Mouse procedures were approved by the Institutional Animal Care and Use Committee of Columbia University. Albino $Rpe65^{rd12}/Rpe65^{rd12}$; $Prkdc^{scid}/Prkdc^{scid}$ mice were used in accordance with the Statement for the Use of Animals in Ophthalmic and Vision Research of the Association for Research in Vision and Ophthalmology, as well as the Policy for the Use of Animals in Neuroscience Research of the Society for Neuroscience.

Cell Culture

Fibroblasts were transduced by lentiviral vectors to create iPS cell lines according to previously established protocols (9). The methods used to induce undifferentiated iPS cells to differentiate into RPE-like cells have been described in detail (10). In brief, iPS cells cocultured with mitomycin-C–treated stromal cells from the PA6 line were transduced with vectors carrying transcription factors *OCT4*, *SOX2*, *KLF4* and *MYC*. The cells were further incubated in differentiation media under 5% CO_2 at 37°C. Differentiation media contain α-minimal essential medium (Gibco; Life Technologies, Carlsbad, CA, USA) supplemented with 15% fetal bovine serum, 40 pmol/L basic fibroblast growth factor (bFGF) (from d 0), 10 nmol/L dexamethasone (from d 3), and 10 pmol/L choleratoxin (only from d 0 to 3). The media were refreshed twice a week. After pigmented cell formation, the pigmented colonies were picked and replated on a PA6 feeder plate in RPE culture medium as previous protocol (11).

Immunocytochemistry

Four antibodies against standard pluripotency markers (TRA-1-60, SSEA4, NANOG and SOX2 [ASK-306, Applied StemCell, Menlo Park, CA, USA]) were applied to characterize the iPS cells reprogrammed from the fibroblasts obtained from a healthy donor. DAPI (4′,6-diamidino-2-phenylindole) was used to stain nuclei. Secondary antibodies conjugated Alexa Fluor 488 goat anti-rabbit or Alexa Fluor 555 goat anti-mouse IgG (1:1,000; Invitrogen; Life Technologies). Images for all antibody labels were taken under the same settings with a fluorescence microscope (Leica DM 5000 B).

Quantitative RT-PCR of Endogenous RPE Biomarkers in Human RPE

RNA was harvested and analyzed by quantitative real-time RT-PCR. Total RNA was isolate from undifferentiated iPS, iPS-derived RPE and human RPE from autopsy. Total cDNA of these samples was reverse transcribed by a superscript III Reverse Transcription Kit (Invitrogen; Life Technologies); oligo-dT was used as a primer. The real-time PCR was then

performed by using primer sets Hs01071462_m1 for RPE65 (4331182), Hs00188249_m1 for bestrophin-1 (4331182) and Hs00363053_g1 for *MFRP* (4331182) (Applied Biosystems; Life Technologies). The mRNA expression level was determined and normalized with hypoxanthine phosphoribosyltransferase 1.

Immunoblot Analysis

After 28 d of iPS differentiation, total cellular protein was extracted and analyzed by sodium dodecyl sulfate–polyacrylamide gel electrophoresis. Samples were then transferred to nitrocellulose membranes. Membranes were incubated with either rabbit anti-RPE65 monoclonal antibody (1:1,000; a gift of T Michael Redmond, National Institutes of Health) or rabbit anti-*CRALBP* monoclonal antibody (1:1,000; Santa Cruz Biotechnology, Santa Cruz, CA, USA). After washing, membranes were further incubated with anti-rabbit–conjugated horseradish peroxidase–conjugated secondary antibodies (1:10,000; Santa Cruz Biotechnology). Blots were detected by chemiluminescence assay (Immobilon Western; EMD Millipore, Billerica, MA, USA). Multiple exposures were obtained using Kodak BioMax film (Kodak, New York, NY, USA) and developed with a Konica medical film processor, SRX-101A (Konica Minolta Medical Imaging USA Inc., Wayne, NJ, USA).

Electron Microscopy

Electron microscopy was performed, according to established protocols. Selected areas were trimmed for ultrathin sectioning and stained with uranyl acetate before electron microscopy observation (12).

Phagocytosis of Photoreceptor Outer Segments

To observe the phagocytosis function of the iPS-derived RPE cells, bovine outer segment extract was added into the supernatant of confluent cell culture as described previously (13). The cells were then incubated at 37°C for 2 h. After incubation, the cells were washed three times with phosphate-buffered saline (PBS) to remove remaining outer segment debris before paraformaldehyde fixation. Double staining was performed using anti-rhodopsin (sc-57432, Santa Cruz Biotechnology) and anti-ZO-1 (40-2200; Zymed;

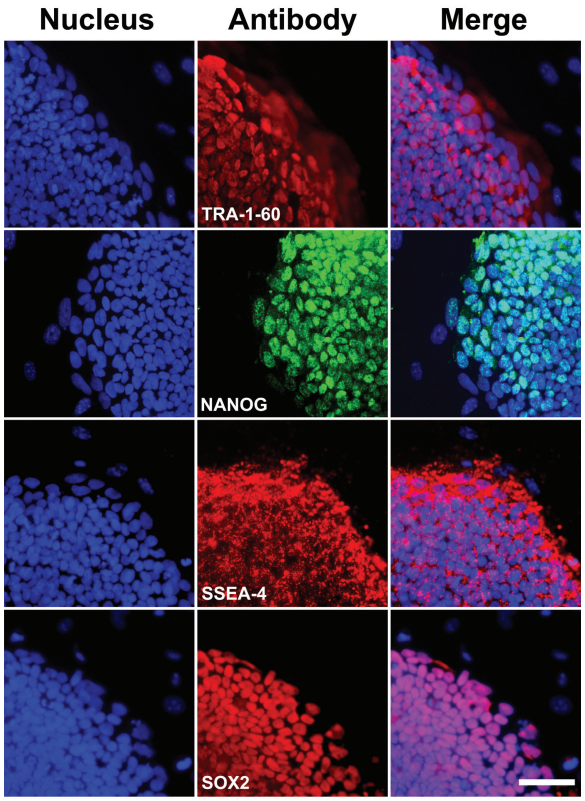

Figure 2. Expression of pluripotency markers in human iPS cells at d 14. Left column: DAPI stained nuclei. Middle column: cells labeled with TRA-1-60, SSEA4, NANOG or SOX2 antibodies; markers of pluripotency. Right column: merged images. Scale bar, 50 μm.

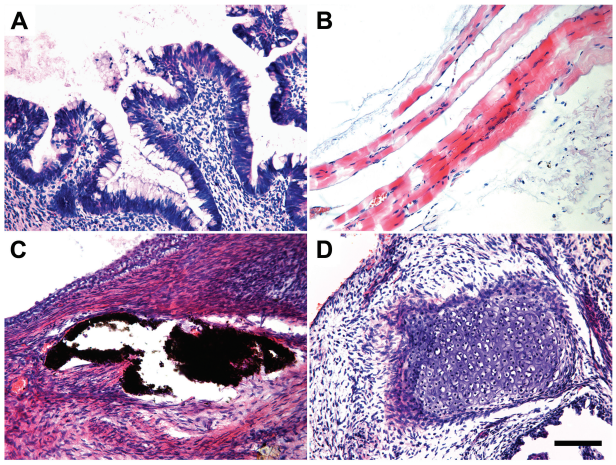

Figure 3. Human iPS cells differentiated into cell types of all three germ layers. (A) Gastrointestinal epithelium (endoderm). (B) Muscle (mesoderm). (C) Neuroepithelium with pigment (ectoderm). (D) Cartilage (mesoderm) (scale bar, 100 μm).

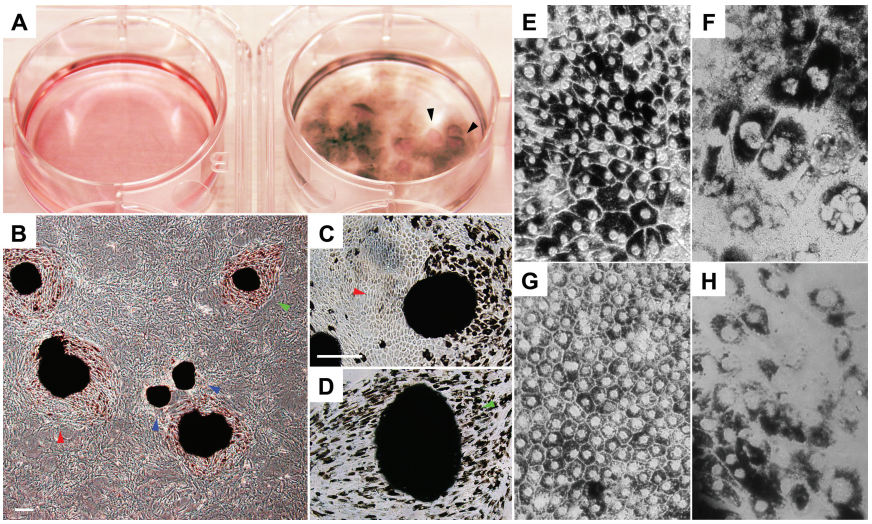

Figure 4. RPE morphology in differentiating human iPS cells. (A) MEF control (left) and differentiated pigmented cells (right). Monolayer cell domes are shown (arrowheads), suggesting apical-basal fluid transportation, an essential function of RPE. (B) Pigmented colonies transferred to feeder plates showing RPE fate. Arrowheads indicate different stages: early (blue), intermediate (red) and mature (green). (C) Colony with mixture of pigmented and nonpigmented hexagonal cells. (D) Colony with most hexagonal cells being pigmented. (E, F) iPS-derived RPE with native RPE morphological characteristics, including prominent melanin granules and perinuclear location of melanin granules. (G, H) Human autopsy RPE. Scale bar, 200 μm.

currently a Life Technologies product) to detect the phagocytosed photoreceptor outer segment (POS) and cell boundary, respectively. The sample was subsequently analyzed by fluorescent microscopy (Leica 5000B, Leica Microsystems, Buffalo Grove, IL, USA).

Subretinal Transplantation

Subretinal injections were perfomed with approximately 1,000 iPS-derived RPE cells, or alternately, mitomycin C–treated undifferentiated mouse ES cells suspended in 1 μL for control eyes. These were injected into the subretinal space of mouse eyes at postnatal d 2 (P2) (10). All mice had ideal bleb detachments at the retinal site of the injection, as judged by postsurgical fundus examination. The contralateral control eye remained uninjected.

Live Imaging

To test transplantation efficiency and graft survival, pigmented human iPS-derived RPE cells were examined in living albino mice by using the Stereo Lumar.V12 (Zeiss, Oberkochen, Germany). We assessed potential infection, inflammation, bleeding or persistent localized retinal detachment after transplantation with a stereomicroscope.

Mice were anesthetized and the corneal surface was covered with Viscotears (Novartis, Basel, Switzerland) with a circular 7.5-mm sapphire window (Edmund Optics, Barrington, NJ, USA). Anesthesia was maintained by a flow of 3% isoflurane in oxygen through a "cone" fitted to the nose of the mouse; eyes were enucleated and placed in 4% paraformaldehyde for 1 h in room temperature and were then be cut into cross-sections.

Histology of the Posttransplanted Eye

After mice were killed, both eyes were enucleated and fixed in 1:2× Karnovsky fixative for 24 h. The eyes were then embedded in paraffin and sectioned at a thickness of 5 microns. Approximately 10–12 sections were collected, containing the optic nerve heads. Retinal sections stained with hematoxylin and eosin were examined by light microscopy (Leica 5000B).

Functional Measurement by ERG

ERGs were conducted until the mice expired at 6 months of age (14). ERG was conducted as described (15). All manipulations were conducted under dim red light illumination, and recordings were made using Espion ERG Diagnosys equipment (Diagnosys LLC, Lowell, MA, USA). Adult C57BL/6 mice were tested at the beginning of each session as controls to make sure both eyes had the same amplitude. Before each ERG recording, iPS-derived RPE grafted $Rpe65^{rd12}/Rpe65^{rd12}$ mice were dark adapted for 12 h and then anesthetized by intraperitoneal injection of 10% ketamine-xylazine-PBS solution. Topical proparacaine, tropicamide (1%) and phenylephrine (2.5%), were used for local anesthesia and pupillary dilation, respectively.

All supplementary materials are available online at www.molmed.org.

RESULTS

Reprogramming Skin Fibroblasts

Fibroblasts were cultured from a skin biopsy taken from a 53-year-old donor (Figure 1A). To create a human iPS cell line, reprogramming was conducted using lentiviral vectors expressing *OCT4*, *SOX2*, *KLF4* and *MYC* (9). Colonies of iPS cells began to appear between 14 and 21 d (Figures 1B–D). Two independent iPS lines were selected for subsequent studies.

Pluripotency Tests of the Human iPS Cell Line

Immunocytochemistry and teratoma assays are established means for scoring stem cell pluripotency. We assessed the expression of membrane bound (TRA-1-81 and SSEA4) and nuclear (NANOG and SOX2) pluripotency markers. Expression of these markers resembled re-

sults seen in native human ES cells (Figure 2). Next, the ability of iPS cells to differentiate into all three germ layers was tested in teratoma assays. Undifferentiated iPS cells were injected into the dorsal flank of *Prkdc*^{scid}/*Prkdc*^{scid} mice subcutaneously. After 8 wks, teratomas generated from the outgrowth of iPS were analyzed by hematoxylin and eosin staining. Within one single teratoma, all three germ-layer tissue types were found (Figures 3A–D), including gastrointestinal epithelium (endoderm), muscle and cartilage (mesoderm) and neuroepithelium with pigment (ectoderm), providing strong evidence for the pluripotency of iPS cells generated with our methods.

Differentiation of Human iPS Cells

To induce RPE differentiation, individual iPS cells were plated on mitomycin-C–treated feeders in 12-well dishes containing differentiation medium (10). After 6 wks of differentiation, approximately 10% of the dishes' surface areas were covered with a layer of cells displaying epithelial morphology, with a large cytoplasmic-to-nuclear ratio. After 12 wks, 30–50% of the surface areas contained cells with pigmented epithelial morphology, and some clusters of cells exhibited fluid domes consistent with fluid transportation from the apical side to the basal side of the cultured monolayer (Figure 4A). Pigmented cells growing in colonies were manually replated onto new dishes with mitomycin-C feeders (Figure 4B). After 7 d, pigmented colonies began to generate nonpigmented cells. Cells assumed a hexagonal epithelial morphological shape typical for RPE. Subsequently, cells began to accumulate pigment after 14 d (Figures 4C, D).

Light Microscopy and Transmission Electron Microscopy (TEM) of Human iPS-Derived RPE Cells

Light and TEM were applied to analyze and compare the morphologies of iPS-derived RPE cells and native human RPE. In light microscopy, hexagonal shape and dark perinuclear melanin granules, which are typical features of RPE, were observed in both iPS-derived RPE cells (Figures 4E, F) and native human fetal RPE (Figures 4G, H). TEM was used for ultrastructure study (Figures 5A–C and D–F). The iPS-derived RPE possessed abundant finger-like microvilli on the outer surface and intercellular space, as seen in native RPE.

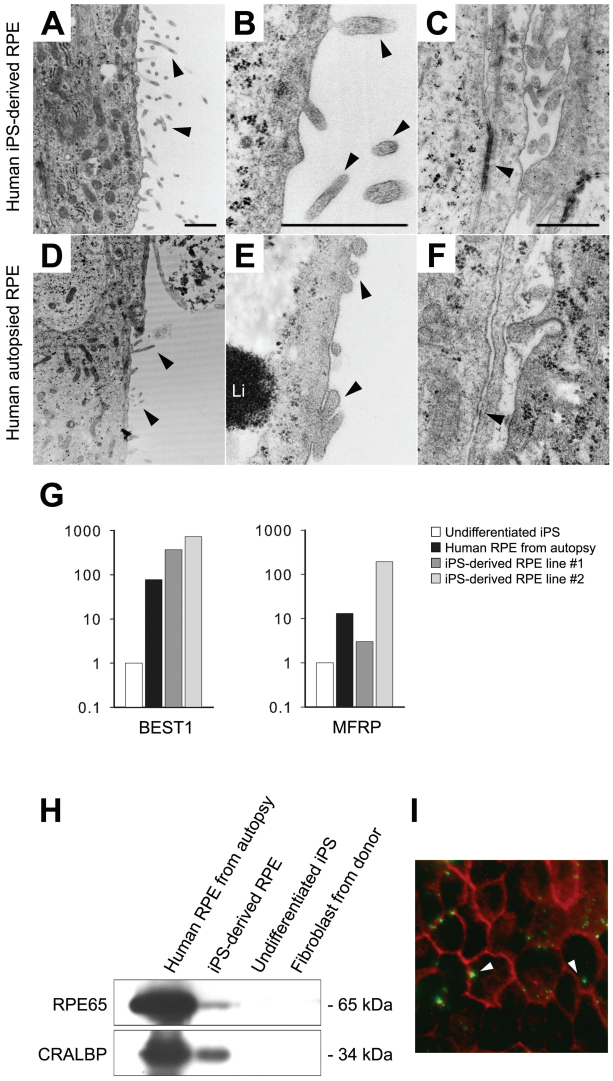

Figure 5. Morphology (A–F), expression (G–H) and functional analyses (I) of our iPS-derived-RPE. Arrowheads indicate apical microvilli (AMv) in iPS-RPE (A, B) and in human autopsy donor RPE (D, E) at 15,000× and 60,000×. Li, lipofusin granule. (C, F) Arrowheads indicate adherens junction-like structure between RPE cells (3,000×). (G) Quantitative RT-PCR of RPE65, BEST1 and MFRP expression in autopsy RP, iPS-RPE, undifferentiated iPS and donor fibroblast. (H) Immunoblot analysis of RPE65 (65 kDa) and CRALBP (34 kDa) expression in autopsy RPE, iPS-RPE, undifferentiated iPS and donor fibroblast. Total protein (20 μg/lane). (I) Phagocytosis of POS in iPS-RPE. Bovine POS (green) and ZO1 (red). White arrowheads indicate POS inside RPE. Scale bar in A–C, 1 μm.

Expression of RPE Makers on iPS-Derived RPE Cells

Quantitative PCR was performed to test the expression of RPE-specific markers, BEST1 and MFRP, in iPS-derived RPE cells (Figure 5G). The transcript levels of two different iPS-derived RPE lines and native human RPE, which served as a positive control, were nor-

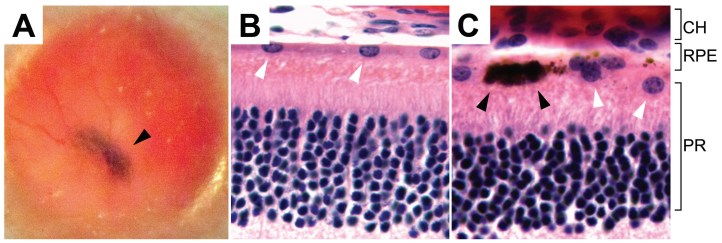

Figure 6. Survival of transplanted iPS-derived pigmented RPE in albino *Rpe65*^{rd12}/*Rpe65*^{rd12} mice. (A) Fundus photograph shows a patch of black pigmented iPS-RPE (arrowhead) behind the albino retinal 5 months after transplantation. No gross disruption of the host retina occurred. (B,C) Histology of host retina 5 months after transplantation. White arrowheads indicate mouse RPE (B). Human pigmented cells, indicated with black arrowheads, are adjacent to the host RPE (C). CH, choroid; PR, photoreceptor.

malized against undifferentiated iPS cells. Both iPS-derived RPE cell lines expressed similar levels of RPE65 and BEST1 compared with native human RPE, whereas one of the iPS-derived RPE lines (#2) expressed a higher level of MFRP (Figure 5G). Immunoblot analysis was performed after 28 d of differentiation *in vitro*. Native RPE-specific markers RPE65 (65 kDa) and CRALBP (34 kDa) were detectable on both human autopsy RPE and iPS-derived RPE but were undetectable on undifferentiated iPS and donor skin fibroblasts (Figure 5H).

Functional Analysis of Human iPS-Derived RPE Cells

Native RPE has the ability to phagocytose photoreceptor outer segments (13). Phagocystosis of photoreceptor outer segments is a common test of native *in vivo* RPE function and is a crucial function provided by RPE. Indeed, the death of RPE cells leads to blindness by causing a buildup of outer segments debris within subretinal space in the RCS rat.

To determine whether iPS-derived RPE would be able to phagocytose outer segments such as native RPE, iPS-derived RPE cells were fed with outer segments isolated from a fresh bovine retina. White arrows point to the outer segments phagocytosed by iPS-derived RPE. Anti-ZO-1 antibody stains the hexagonal RPE cell borders (Figure 5I).

Tumorigenesis and Posttransplant RPE Survival

Our previous studies showed evidence of tumor formation around 3 wks after ES transplantation (10). In the present study, we injected 34 mice (see below) with iPS-derived RPE, and none developed gross tumors in their lifetime. Furthermore, serial histological sections on seven globes did not detect microscopic tumor formation. Fundoscopy photography confirmed the presence of pigment grafts at the mid-peripheral and peripheral retinas at three intervals (Figure 6A). Histological sections from a 5-month-old albino *Rpe65*^{rd12}/*Rpe65*^{rd12} mouse confirmed the presence and survival of iPS-derived RPE tissue after transplant into the subretinal space. The host RPE and iPS-derived RPE cells colocalized between the choroid and photoreceptor layer (Figures 6B–D). Histology confirmed formation of a new RPE layer interspersed with pigmented human RPE and albino RPE. Albino host cells were seen integrated among human pigmented cells with no apparent disruption in the host RPE layer, suggesting successful incorporation of iPS-derived RPE.

ERG Activity Was Restored in a Preclinical Model for RP after iPS-Derived RPE Transplantation

Our previous studies with an RP mouse model (*Rpe65*^{rd12}/*Rpe65*^{rd12}) demonstrated fetal mouse RPE- or ES-derived RPE grafts can restore retinal function (10,16). To test human iPS-derived RPE, we bred *Rpe65*^{rd12}/*Rpe65*^{rd12} and *Prkdc*^{scid}/*Prkdc*^{scid} (SCID) to generate double homozygotes; the SCID phenotype reduces the possibility of graft versus host disease. After subretinal injections of RPE cells into the right eye of 34 newborn mice, we monitored mice for differences in ERG responses between injected right eyes and uninjected left eyes; experiments were terminated after 6 months, since SCID mice rarely survive beyond 7–8 months.

Among the 34 mice receiving human iPS-derived RPE transplantation, we were able to analyze ERG responses in both eyes of 24 mice, since the right eyes of 10 mice showed obvious signs of retinal detachment or the ERGs were severely extinguished. Suspected surgical trauma was also detected in 17 of the remaining 24 mice, since the right eye maximum b-wave amplitudes were at least two standard deviations below those of the left control eye (Supplementary Figures S1, S2). Normally, in untreated *Rpe65*^{rd12}/*Rpe65*^{rd12} mice, there is no significant interocular asymmetry detectable in untreated right and left eye pairs (Supplementary Figure S1). We then analyzed the ERGs of the remaining seven treated mice (Figure 7). An example of ERG traces for treated and control eyes compared with a wild-type response is shown (Figure 7A). The average b-wave peak difference between treated and control eyes was measured as 13.7 μV, which was significant (ratio-paired *t* test, $p = 0.0246$, n = 7) (Figure 7B).

As a transplantation control, ERG readings were measured in *Rpe65*^{rd12}/*Rpe65*^{rd12} mice grafted with mitomycin-C–treated ES cells from C57BL/6 mice. Right eyes were injected, whereas fellow left eyes were left untouched. ERGs were performed on all treated and control eyes simultaneously. Six *Rpe65*^{rd12}/*Rpe65*^{rd12} mice without surgical trauma failed to show statistically significant changes in ERG responses ($p = 0.2853$, n = 6) (Figure 7B).

DISCUSSION

RPE maintains the function of light-sensing photoreceptor neurons. Death of RPE leads to degeneration of the light-sensing neurons and vision loss, which affects the ability to perform daily tasks and may lead to depression. About 20% of Americans between the ages of 65 and 75 years can expect to experience RPE loss, an incidence that will double in this decade. As the current study attempts to show, transplantation of iPS-derived RPE cells has the potential to restore lost vision in humans and preclinical models of RPE loss. We tested this ability in the *Rpe65*^{rd12}/*Rpe65*^{rd12} mouse by using ERG readings and found that vision improved after injection with iPS-derived RPE. Our studies provide evidence for the preclinical feasibility of bringing autologous stem cell transplantation into a phase I/II clinical trial for patients with RPE diseases.

Because of the well-known risks of tumorigenesis associated with reprogramming, our current study extended our previous RPE differentiation protocol (10). The risk of tumorigenesis associated with iPS differentiation was attributed to a portion of the iPS cells remaining undifferentiated at the end of the reprogramming protocol. Our extended protocol may have contributed to the lack of tumor formation in the present study. These results support the safety of iPS cells for autologous transplantation. We also confirmed the integration of iPS-derived RPE by host retinas. After transplantation, histology revealed RPE was able to adapt to host tissues; no detectable disruption of albino host cells was observed.

Electrophysiological testing provided evidence that iPS-derived RPE grafts can support neuronal function in *Rpe65*^{rd12}/*Rpe65*^{rd12} mice. Previously, we demonstrated the recovery of visual function in this preclinical model after fetal RPE (16) and ES cell transplantation (10). To ensure these iPS-derived RPE cells were not rejected, we used SCID *Rpe65*^{rd12}/*Rpe65*^{rd12} mice, which typically die at 7 or 8 months of age, as recipients (14). After transplantation, ERGs were conducted up to 6 months, covering 75–85% of the lifetime of the SCID mice. To minimize all other sources of variability, mice used in the study were all littermates; to test the therapy efficacy of iPS-derived RPE, transplantation and ERGs were performed concomitantly for all of the mice in the study, and we compared the ERG results between transplanted and fellow eyes of each mouse independently.

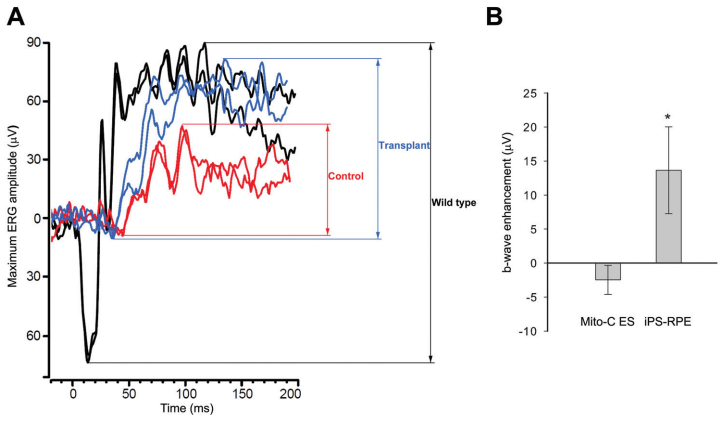

Figure 7. Retinal function is restored in *Rpe65*^{rd12}/*Rpe65*^{rd12} in SCID mice after human iPS cell–derived RPE transplantation. (A) Representative maximum ERG traces from treated (blue), control fellow eye (red) and wild-type mice (black). (B) Maximal b-wave peak analysis. Enhancement is calculated as the difference in maximum responses between treated and untreated control eyes. iPS-RPE–treated eyes show a 13.7-μV average difference (*p = 0.0246, n = 7). Mice receiving mitomycin-C–treated ES cells (mito-C ES) failed to show any statistically significant differences (p = 0.2853, n = 6). The value is represented as the mean ± standard error of the mean, and the p value is conducted by a ratio-paired t test.

Confounding effects of the surgery-induced rescue described in the RCS rat (17–22) were avoided as much as possible by the study of mitomycin-C–treated stem cell grafts as control groups. In previous studies of iPS-derived RPE in the RCS rat, iPS transplantation was shown to produce a rescue effect on optokinetic behavior but not ERG function (6). The RCS rat has a defective MerTK receptor tyrosine kinase that halts phagocytosis within RPE cells and leads lipofuscin to accumulate in the subretinal space, finally leading to the death of photoreceptors before 3 months of age (17–22). Rescue via transplantation with either a human immortal RPE cell line (ARPE-19) (19–22) or native RPE cells (4,5) has been achieved in the RCS rat model. Remarkably, "saline injections" produced a similar efficacy lasting up to a period of 6 months in RCS rats (19–22). Improvement may have been due to the effects of the saline in washing outer segment debris from the subretinal space.

Our present study attempted to differentiate between the effects of the surgical injury–induced rescue from cell transplantation by studying control groups grafted with mitomycin-C–treated undifferentiated ES cells. The ERGs from mice in the control groups showed no statistically significant differences between transplanted and control fellow eyes, whereas the ERGs from mice transplanted with iPS-derived RPE cells showed statistically significant improvement in transplanted but not control fellow eyes. The relatively small absolute (but significant) improvement in the ERG reflects the small size of the transplanted area.

CONCLUSION

In summary, our studies indicate that differentiated iPS cells express RPE-specific markers and provide evidence

that iPS cells have the potential to differentiate morphologically and functionally into RPE. Our study results demonstrate that retinal function can be restored and that iPS cell derivatives integrate functionally into the degenerating *Rpe65*^{rd12}/*Rpe65*^{rd12} retina. ERG recordings show that transplanted iPS-derived RPE cells can restore neuronal function in a preclinical model of RP. The implications of this are promising, since autologous iPS transplantation may restore lost vision and provide treatment for advanced stages of RP and AMD featuring significant RPE loss.

ACKNOWLEDGMENTS

We thank Chyuan-Sheng Lin, Takayuki Nagasaki and Kristy Brown for technical assistance; Haiqing Hua for experimental guidance and advice and Scott Noggle and the New York Stem Cell Foundation Laboratory for support. This study was supported by the Joan and Michael Schneeweiss Research Fund. Y Li's research is supported by NYSTEM grant C026448. The Bernard and Shirlee Brown Glaucoma Laboratory is supported by core grants 5P30CA013696, P30EY019007, R01EY018213 and TS080017-W81XWH-09-1-0575 (all four from NIH); Research to Prevent Blindness and the Foundation Fighting Blindness. SH Tsang is a fellow of the Burroughs-Wellcome Program in Biomedical Sciences and has been supported by the Bernard Becker Association of University Professors in Ophthalmology, Research to Prevent Blindness, the Foundation Fighting Blindness, the Dennis W. Jahnigen Award of the American Geriatrics Society, Joel Hoffman Fund, Gale and Richard Siegel Stem Cell Fund, Charles Culpeper Scholarship, Irma T. Hirschl Charitable Trust, Bernard and Anne Spitzer Stem Cell Fund, Barbara and Donald Jonas Family Fund and Professor Gertrude Rothschild Stem Cell Foundation.

DISCLOSURE

The authors declare that they have no competing interests as defined by *Molecular Medicine*, or other interests that might be perceived to influence the results and discussion reported in this paper.

REFERENCES

1. Rosenfeld PJ, *et al.* (2006) Ranibizumab for neovascular age-related macular degeneration. *N. Engl. J. Med.* 355:1419–31.
2. Schwartz SD, *et al.* (2012) Embryonic stem cell trials for macular degeneration: a preliminary report. *Lancet.* 379:713–20.
3. Buchholz DE, *et al.* (2009) Derivation of functional retinal pigmented epithelium from induced pluripotent stem cells. *Stem Cells.* 27:2427–34.
4. Yamamoto S, Du J, Gouras P, Kjeldbye H. (1993) Retinal pigment epithelial transplants and retinal function in RCS rats. *Invest. Ophthalmol. Vis. Sci.* 34:3068–75.
5. Lopez R, *et al.* (1989) Transplanted retinal pigment epithelium modifies the retinal degeneration in the RCS rat. *Invest. Ophthalmol. Vis. Sci.* 30:586–8.
6. Carr AJ, *et al.* (2009) Protective effects of human iPS-derived retinal pigment epithelium cell transplantation in the retinal dystrophic rat. *PLoS One.* 4:e8152.
7. Berson EL. (1993) Retinitis pigmentosa: The Friedenwald Lecture. *Invest. Ophthalmol. Vis. Sci.* 34:1659–76.
8. Berson EL. (2007) Long-term visual prognoses in patients with retinitis pigmentosa: the Ludwig von Sallmann lecture. *Exp. Eye Res.* 85:7–14.
9. Lin T, *et al.* (2009) A chemical platform for improved induction of human iPSCs. *Nat. Methods.* 6:805–8.
10. Wang NK, *et al.* (2010) Transplantation of reprogrammed embryonic stem cells improves visual function in a mouse model for retinitis pigmentosa. *Transplantation.* 89:911–9.
11. Maminishkis A, *et al.* (2006) Confluent monolayers of cultured human fetal retinal pigment epithelium exhibit morphology and physiology of native tissue. *Invest. Ophthalmol. Vis. Sci.* 47:3612–24.
12. Tsang SH, *et al.* (1996) Retinal degeneration in mice lacking the gamma subunit of the rod cGMP phosphodiesterase. *Science.* 272:1026–9.
13. Ryeom SW, Sparrow JR, Silverstein RL. (1996) CD36 participates in the phagocytosis of rod outer segments by retinal pigment epithelium. *J. Cell Sci.* 109:387–95.
14. Bosma MJ, Carroll AM. (1991) The SCID mouse mutant: definition, characterization, and potential uses. *Annu. Rev. Immunol.* 9:323–50.
15. Davis RJ, *et al.* (2008) Functional rescue of degenerating photoreceptors in mice homozygous for a hypomorphic cGMP phosphodiesterase 6 b allele (Pde6bH620Q). *Invest. Ophthalmol. Vis. Sci.* 49:5067–76.
16. Gouras P, Kong J, Tsang SH. (2002) Retinal degeneration and RPE transplantation in Rpe65(-/-) mice. *Invest. Ophthalmol. Vis. Sci.* 43:3307–11.
17. Silverman MS, Hughes SE. (1990) Photoreceptor rescue in the RCS rat without pigment epithelium transplantation. *Curr. Eye Res.* 9:183–91.
18. Faktorovich EG, Steinberg RH, Yasumura D, Matthes MT, LaVail MM. (1990) Photoreceptor degeneration in inherited retinal dystrophy delayed by basic fibroblast growth factor. *Nature.* 347:83–6.
19. Schraermeyer U, *et al.* (2001) Subretinally transplanted embryonic stem cells rescue photoreceptor cells from degeneration in the RCS rats. *Cell Transplant.* 10:673–80.
20. Grisanti S, *et al.* (2002) Xenotransplantation of retinal pigment epithelial cells into RCS rats. *Jpn. J. Ophthalmol.* 46:36–44.
21. Sauve Y, Girman SV, Wang S, Keegan DJ, Lund RD. (2002) Preservation of visual responsiveness in the superior colliculus of RCS rats after retinal pigment epithelium cell transplantation. *Neuroscience.* 114:389–401.
22. Wang S, *et al.* (2008) Morphological and functional rescue in RCS rats after RPE cell line transplantation at a later stage of degeneration. *Invest. Ophthalmol. Vis. Sci.* 49:416–21.